Journal of the European Ceramic Society 17 (1997) 1301–1308
© 1997 Elsevier Science Limited
Printed in Great Britain. All rights reserved
PII: S0955-2219(96)00238-5
0955-2219/97/$17.00

β-Si_3N_4 Grain Growth, Part II: Intergranular Glass Chemistry

H. Björklund and L. K. L. Falk*

Department of Physics, Chalmers University of Technology, S-412 96 Göteborg, Sweden

(Received 16 August 1996; revised version received 7 November 1996; accepted 11 November 1996)

Abstract

The intergranular chemistry and the substitution level of the β′-grains in a Si_3N_4 ceramic fabricated with 9·5 mol% Al_2O_3 and Y_2O_3 have been characterised by high resolution analytical transmission electron microscopy. The Y_2O_3/Al_2O_3 molar ratio of the starting powder mixture corresponded to that of the Y,Al-garnet ($5Al_2O_3{\cdot}3Y_2O_3$). Al and O were incorporated into the Si_3N_4 structure during densification and a dilute β′-Si_3N_4 formed. Al concentration gradients were not observed in the β′-grains, although the Al substitution level varied within and between β′-grains ($0{\cdot}16 \leq z \leq 0{\cdot}24$). The consequently reduced Al content of the oxynitride liquid phase sintering medium resulted in a limited formation of N-α-wollastonite (Y_2SiAlO_5N) during cooling from the densification temperature. Y and Al were not homogenously distributed in the residual glass pockets; an enrichment close to the β-Si_3N_4 grains could be observed. Both Y and Al were observed also in the glassy films between adjacent β′-grains. Growth ledges on $\{10\bar{1}0\}$ facets of β′-grains facing curved grain boundaries resulted in a variation of the intergranular film thickness. These features are consistent with grain growth by coalescence. © *1997 Elsevier Science Limited.*

1 Introduction

Quantitative microscopy of Si_3N_4 ceramics fabricated with a constant molar fraction of the metal oxide additives Al_2O_3 and Y_2O_3 or Yb_2O_3 has shown that the combination of additives as well as the time at densification temperature has a crucial influence on β-Si_3N_4 grain morpholgy and the intergranular microstructure.[1] An increased Y_2O_3/Al_2O_3 molar ratio of the starting powder mixture resulted in a higher average aspect ratio and also in a larger mean grain size after shorter times at the densification temperature. This effect of the Y_2O_3/Al_2O_3 ratio on grain size seemed, however, to level out with a prolonged densification time. Reconstructed three-dimensional grain size distributions implied that the β-Si_3N_4 grain growth was rate controlled by diffusion through the liquid phase sintering medium. Scanning electron microscopy (SEM) of polished and etched sections suggested that grain growth primarily occurred by coalescence.

The oxynitride liquid phase sintering medium forms through reaction between the metal oxide sintering additives, the inherent surface silica present on the Si_3N_4 starting powder particles and some of the Si_3N_4.[2–4] The α-Si_3N_4 in the starting powder compact is preferentially dissolved in the liquid, and β-Si_3N_4 will initially precipitate either homogenously in a supersaturated liquid or on pre-existing β-particles. The β-Si_3N_4 grains will adopt a shape close to that of a hexagonal prism if they are allowed to grow without steric hindrance in a suitable liquid environment,[5] (Fig. 1). This shape reflects the hexagonal crystal structure, and the *c*-axis is in the length direction of the grain. Secondary crystalline phases may partition from the liquid phase sintering medium, but a certain fraction is generally retained as a residual intergranular glass in the Si_3N_4 microstructure. Larger volumes of residual glass may, in some systems, be crystallised during a post-densification heat treatment.[6]

The detailed microstructure and microchemistry of sintered materials have to be determined in order to characterise the influence of liquid phase chemistry on β-Si_3N_4 grain growth. The present investigation is concerned with high resolution microanalysis of a Si_3N_4 material fabricated with the addition of 5·9 mol% Al_2O_3 and 3·6 mol% Y_2O_3.

2 Experimental

2.1 Experimental material

The Si_3N_4 powder (E-10 grade, Ube Industries Ltd, Japan) was mixed with Y_2O_3 (Y-F grade,

*To whom correspondence should be addressed.

Mitsubishi Kasei Co., Japan) and Al_2O_3 (AKP-30 grade, Sumitomo Electric, Japan). The oxygen content of the Si_3N_4 starting powder corresponds to 5·6 mol% SiO_2. The total molar fraction of metal oxide additives was 9·5 mol% and the Y_2O_3/Al_2O_3 molar ratio corresponded to that of the Y,Al-garnet (YAG), $5Al_2O_3{\cdot}3Y_2O_3$.

Densification was performed by gas pressure sintering (GPS) with a final densification temperature of 1900°C under a nitrogen pressure of 980 kPa. The specimen was held at 1900°C for 5 h. Detailed descriptions of the powder processing and the densification process are given in Ref. 1.

X-ray diffraction (XRD) showed that the α-Si_3N_4 in the starting powder had completely transformed to β-Si_3N_4.[1] A secondary crystalline phase, Al-substituted N-α-wollastonite (Y_2SiAlO_5N), was also identified. Wollastonite is formed by glass devitrification during cooling from the densification temperature and is not stable at temperatures above 1100°C.[7]

The general microstructure of the experimental material has been characterised by scanning electron microscopy (SEM) of polished and etched sections,[1] (Fig. 2(a)). The three-dimensional β-Si_3N_4 grain size distribution was reconstructed from the SEM images by quantitative microscopy and a stereological method. This showed that the microstructure was fibrous with an average β-Si_3N_4 grain aspect ratio of 3, and that the experimental material had a broad grain size distribution with a certain fraction of larger β-grains (see Fig. 2(b)).

2.2 High resolution microanalysis

The fine-scale microstructure was characterised by transmission electron microscopy (TEM) using a Philips CM 200 SuperTwin microscope with a field emission gun (FEG). The FEG TEM is equipped with a Link ISIS system for quantitative energy dispersive X-ray analysis (EDX).

Local cation concentrations were determined by EDX analysis using a probe with a nominal full width at half maximum (FWHM) of around 1 nm. Cation concentration profiles were obtained by point analysis in steps of 5 or 7·5 nm. Quantitative EDX analysis was carried out using the Link ISIS TEMQuant software with absorption correction and the standard profiles and K_{xSi} values supplied by Link.

Thin foils for TEM were prepared by standard techniques and final thinning was obtained by ion milling. A thin carbon film was evaporated on to the specimen in order to avoid charging in the TEM.

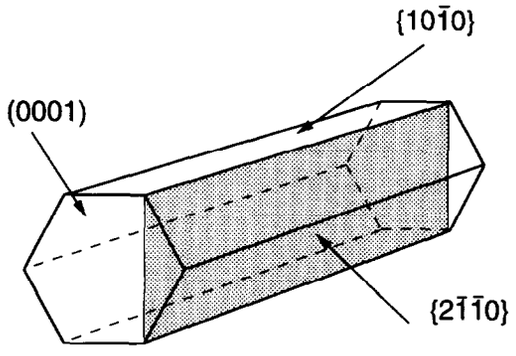

Fig. 1. The idealised β- or β'-Si_3N_4 grain shape. The end surfaces of the hexagonal prism are in the (0001) crystallographic plane and the sides of the prism are the {10$\bar{1}$0} planes.

3 Results

3.1 General microstructure

Intergranular pockets contained either the Al-substituted α-wollastonite or a Y- and Al-rich glassy phase. There was no obvious difference in the size between glassy and crystalline pockets. Microanalysis was concentrated to the glassy regions since the glass is the residue of the liquid

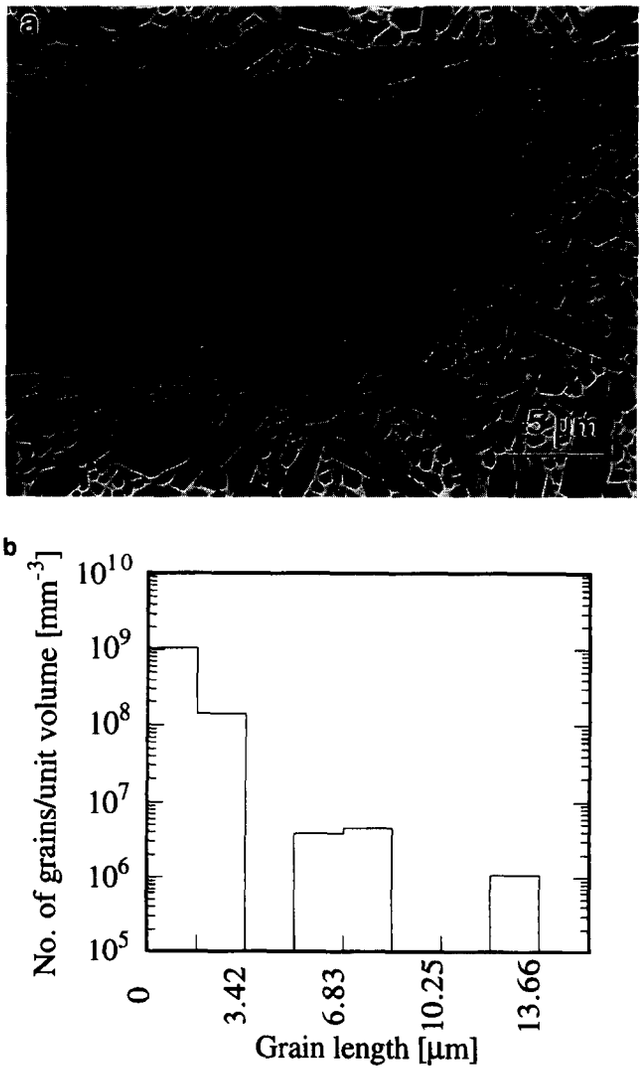

Fig. 2. SEM image of (a) a plasma-etched section of the experimental material and (b) the β'-Si_3N_4 grain size distribution reconstructed with quantitative microscopy and a stereological method.[1]

phase sintering medium, and the wollastonite forms from glass pockets of suitable composition and size at comparatively low temperatures during cooling. The relatively low Y content of the glass, generally less than 20 at%, can be explained by the local formation of the Y-rich α-wollastonite, Y_2SiAlO_5N. The duplex intergranular microstructure also indicates an inhomogeneous distribution of the metal oxide sintering additives.

The typical microstructure of a region containing pockets of residual glass is shown in Fig. 3. Selected area electron diffraction from faceted β-Si_3N_4 grain sections showed that the β-grains had a prismatic shape with planar $\{10\bar{1}0\}$ grain facets when allowed to grow freely in the liquid environment (Figs 4 and 5). The interfaces in the

Fig. 3. Bright field TEM image of the microstructure where glass pockets (arrowed) are present. Steric hindrance of larger β′-grains can be observed.

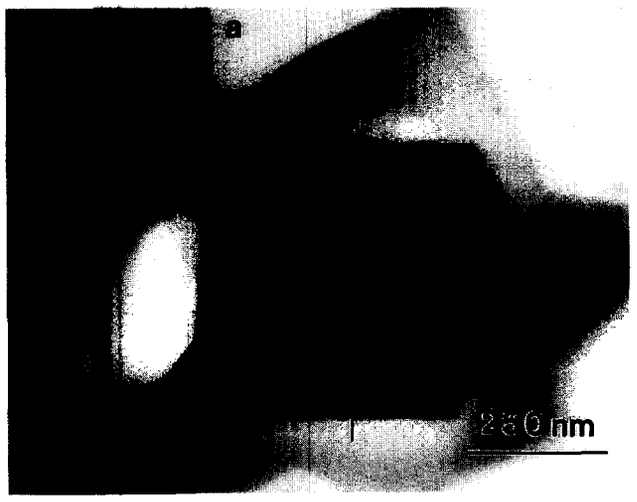

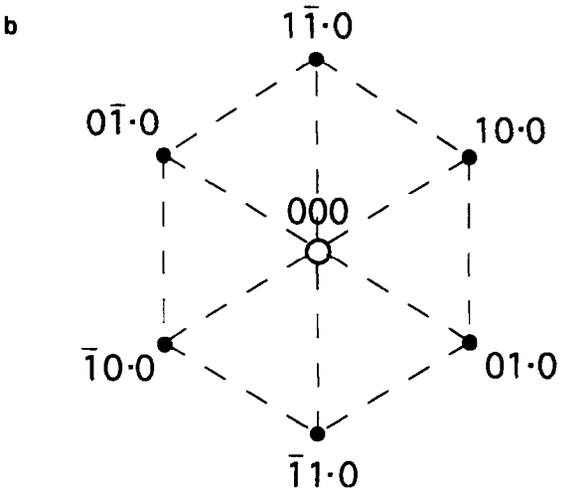

Fig. 4. (a) Bright field TEM image of a nearly hexagonal β′-Si_3N_4 grain cross-section. One of the corners is rounded due to impingement on an adjacent grain. The inserted electron diffraction pattern shows that the direction of the incoming electron beam was [0001] (i.e. along the *c*-axis of the lattice). The line shows the location of the concentration profile in Fig. 7. (b) Indexed diffraction pattern.

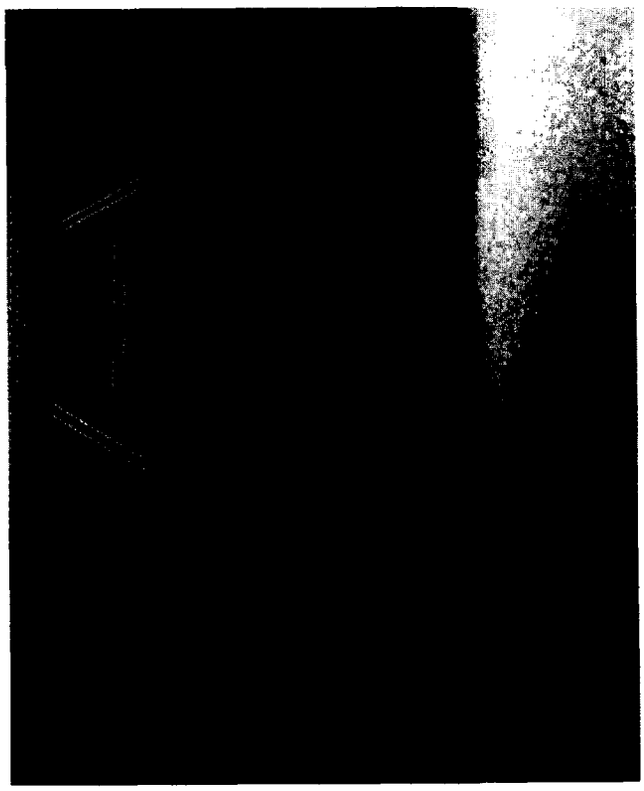

Fig. 5. (a) Bright field TEM image of a cross-section of a β′-grain. The line shows the location of the concentration profile in Fig. 8. (b) High resolution image of the investigated area which shows that the direction of the incoming electron beam was [0001]. The lattice fringes correspond to the three sets of $\{10\bar{1}0\}$ planes with a spacing of 0·66 nm.

[0001] direction of the β-Si_3N_4 grains were generally quite irregular due to contact with other β-grains (Fig. 3). Only a few β-Si_3N_4 grains with a free growth front in the [0001] direction facing glass pockets were observed. It can be noted that also these interfaces were rounded (Fig. 6).

3.2 β-Si_3N_4 and glass chemistry

EDX analysis showed that the β-Si_3N_4 grains had dissolved smaller amounts of Al. β-Si_3N_4 may incorporate Al and O during growth in an oxynitride liquid phase environment and form β'-Si_3N_4 with composition $Si_{6-z}Al_zO_zN_{8-z}$ where $z \leq 4{\cdot}2$.[8] The z values in the present material were determined to be in the range 0·16 to 0·24. EDX profiles across grain boundaries and grains did not show any concentration profiles in the β'-grains, although the local Al substitution within a grain varied (Fig. 7).

Concentration profiles across edge on $\{10\bar{1}0\}$ prism sides facing larger glass volumes, are shown in Figs 7 and 8. The β'-Si_3N_4 grains were oriented with the hexagonal c-axis (the crystallographic [0001] direction) parallel to the electron beam. These concentration profiles showed that the cations were not homogeneously distributed in the

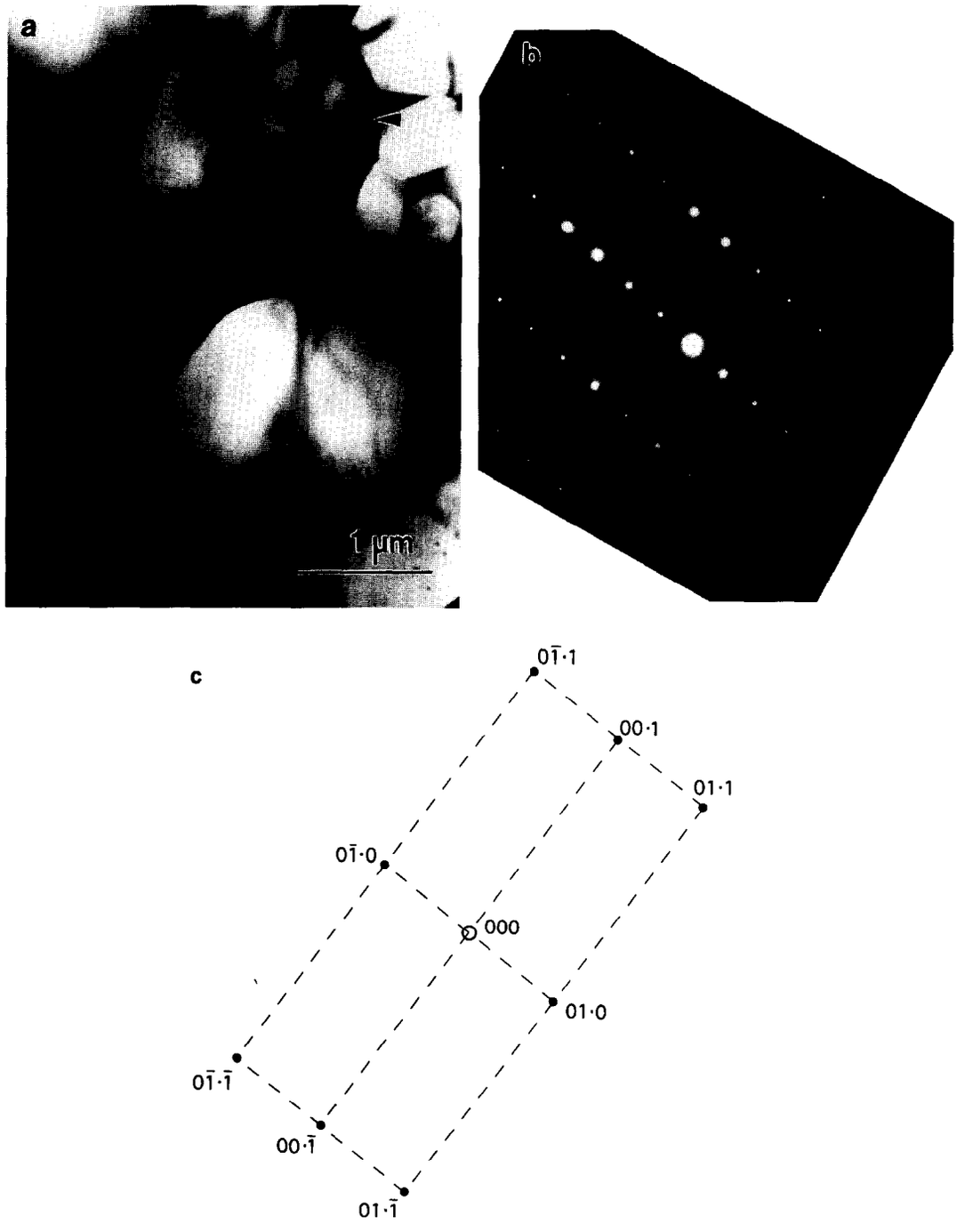

Fig. 6. (a) β'-Si_3N_4 growth front in the [0001] direction facing a glass pocket (arrow). (b) The selected area electron diffraction pattern from the β'-grain shows that the direction of the electron beam was $[2\bar{1}\bar{1}0]$ and that the β'-grain length axis (the [0001] direction) is perpendicular to the incoming electron beam. (c) Indexed electron diffraction pattern.

amorphous phase. The profiles showed an enrichment of Y and Al at a distance of 5–30 nm from the prism side; these concentrations decreased at larger distances from the β′-grain. The Y/Al ratio of the glass was sometimes comparatively low close to the β′-grain but increased to a relatively constant value at distances > 10 nm (Figs 7(b) and 8(b)). The Y/Al ratios then fluctuated around a value which was between 1·5 and 2·4 further away from the β′-grain facet.

Concentration profiles across β′-Si_3N_4 growth fronts in the [0001] direction into glass pockets also showed an enrichment of Y and Al close to the rounded interface. These concentration profiles were obtained from β′-Si_3N_4 grains with the [2$\bar{1}\bar{1}$0] crystallographic direction parallel to the electron beam (Fig. 9). The β′-Si_3N_4 *c*-axis ([0001] direction) was then perpendicular to the electron beam and in the length direction of the grain section as shown by selected area electron diffraction. Figure 10 shows a concentration profile across a β′-Si_3N_4 curved interface, across the adjacent glass pocket and into another β′-grain facing the glass. There was an Y and Al enrichment close to both β′-grains. The rounded interface of the first β′-grain resulted in a slight overlap with the glass (i.e. the boundary was slightly curved also in the beam direction) and detection of Y and Al from the glass resulted in the anomalous profile in this β′-grain close to the glass pocket. The Y/Al ratio was relatively constant in the centre of the glass pocket (Fig. 10(b)).

3.3 Intergranular films

Adjacent β-Si_3N_4 grains were separated by intergranular amorphous films (see Figs 9(b), 11 and 12). EDX point analysis of the grain boundary films showed that they contained Al and Y.

Ledges at β′-grain surfaces facing curved grain boundaries resulted in a variation in grain boundary film thickness (see Figs 11 and 12). The observed ledges were present on {10$\bar{1}$0} grain facets, and the film thickness was in one case (Fig. 12) determined to vary between 0·7 and 1·5 nm using the {10$\bar{1}$0} lattice fringes, which correspond to an interplanar spacing of 0·66 nm, as internal standard. Concentration profiles across curved grain boundaries showed an enrichment of Y and Al also to these glassy intergranular films, (Fig. 13).

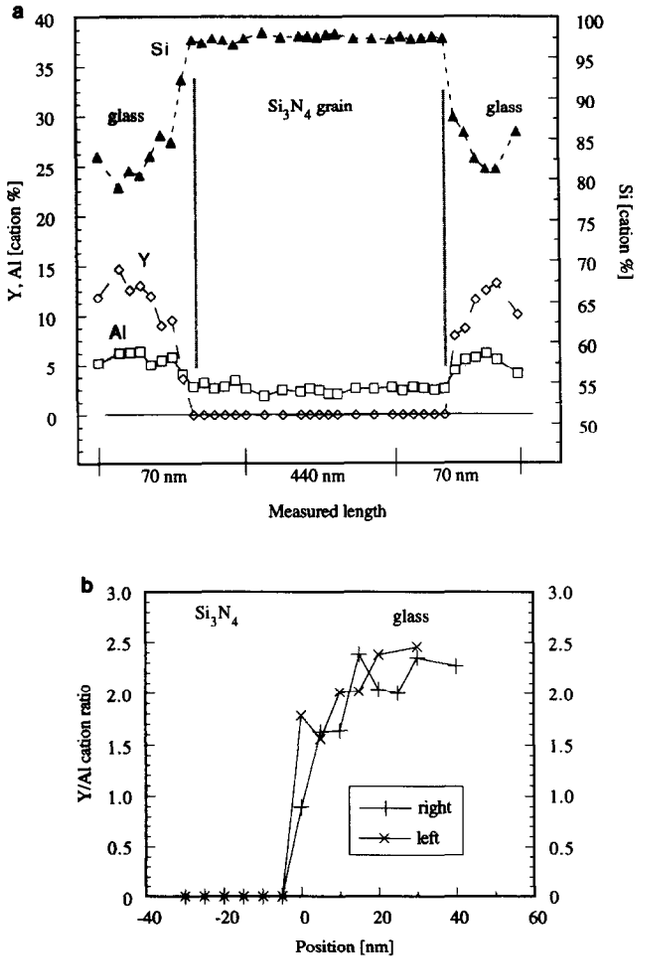

Fig. 7. (a) Cation concentration profiles across the β′-Si_3N_4 grain in Fig. 4. (b) Y/Al cation ratios in the two glass pockets; right and left refer to the profiles in (a).

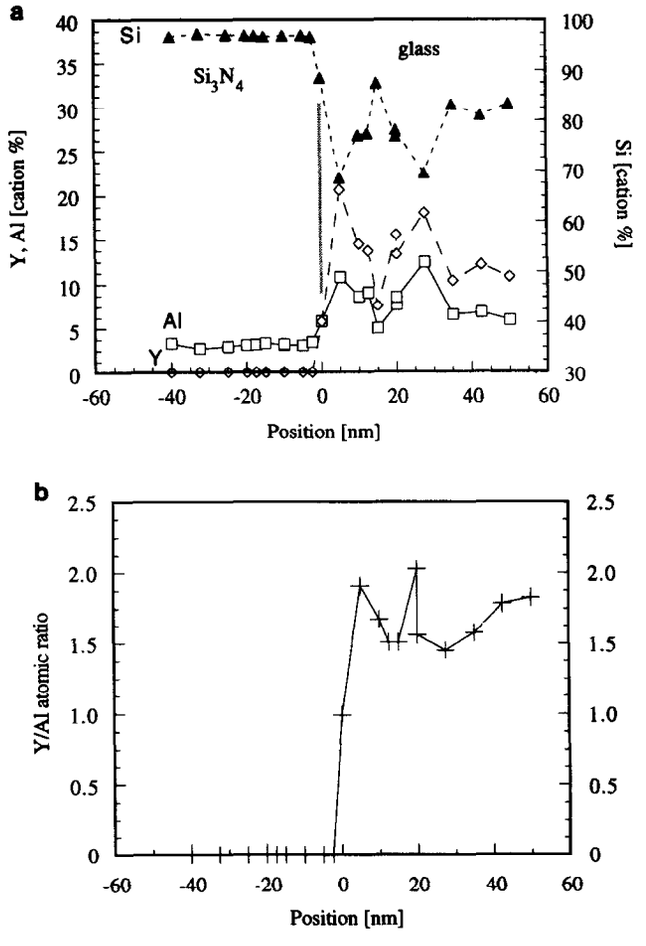

Fig. 8. (a) Cation concentration profiles across an edge on {10$\bar{1}$0} facet in Fig. 5. (b) Y/Al cation ratio profile. These profiles were obtained from two measurements, one in steps of 5 nm and one in steps of 7·5 nm.

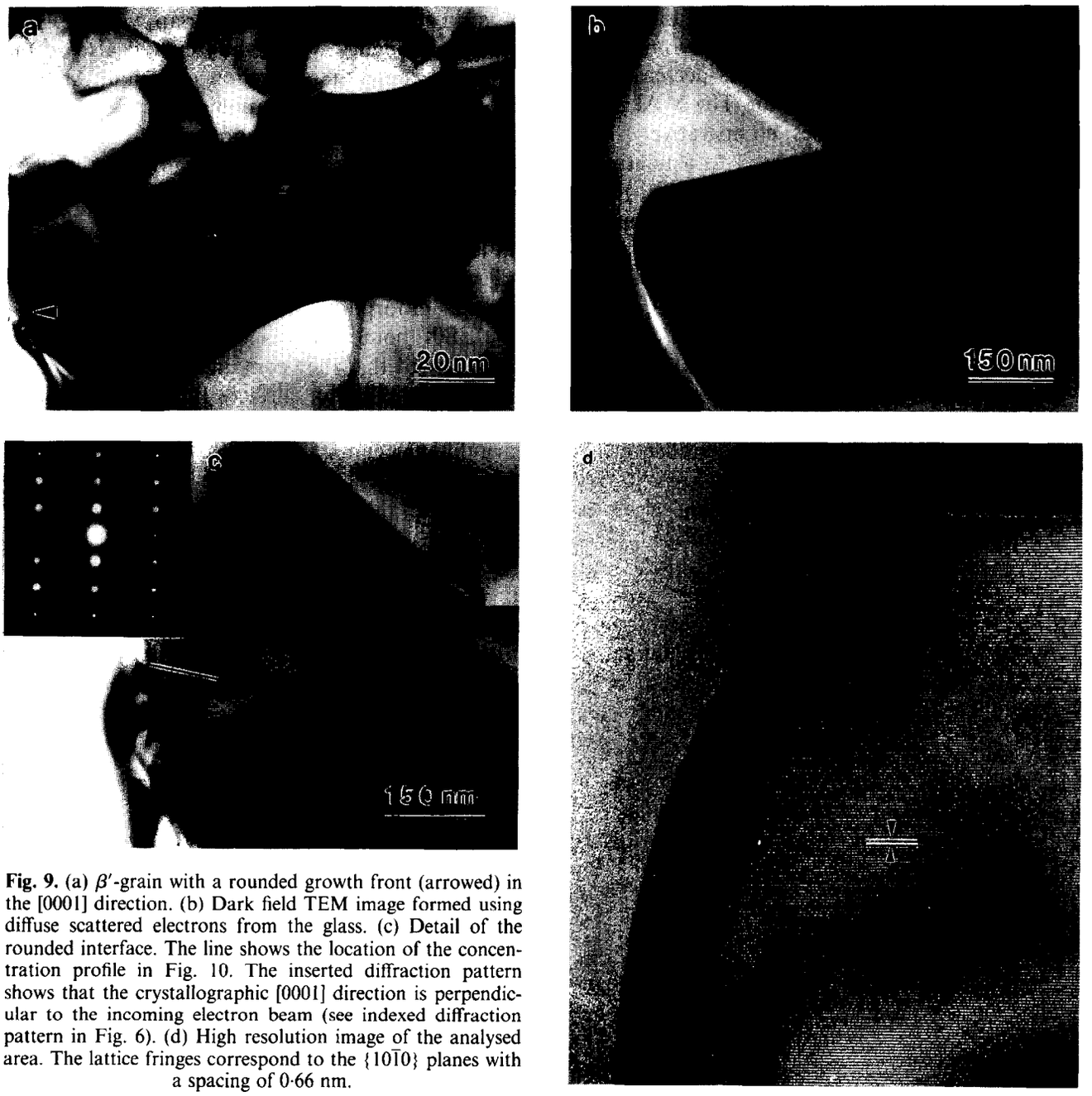

Fig. 9. (a) β'-grain with a rounded growth front (arrowed) in the [0001] direction. (b) Dark field TEM image formed using diffuse scattered electrons from the glass. (c) Detail of the rounded interface. The line shows the location of the concentration profile in Fig. 10. The inserted diffraction pattern shows that the crystallographic [0001] direction is perpendicular to the incoming electron beam (see indexed diffraction pattern in Fig. 6). (d) High resolution image of the analysed area. The lattice fringes correspond to the $\{10\bar{1}0\}$ planes with a spacing of 0·66 nm.

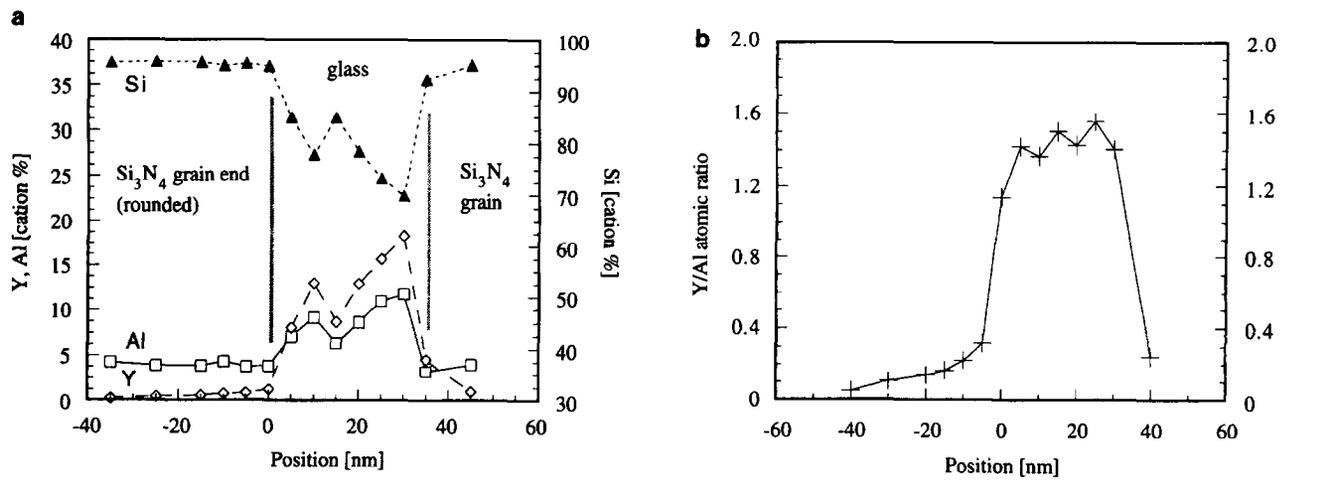

Fig. 10. (a) Cation concentration profiles across the rounded interface of the β'-grain, across the glass pocket and into the opposite β'-grain in Fig. 9. (b) Y/Al cation ratio profile.

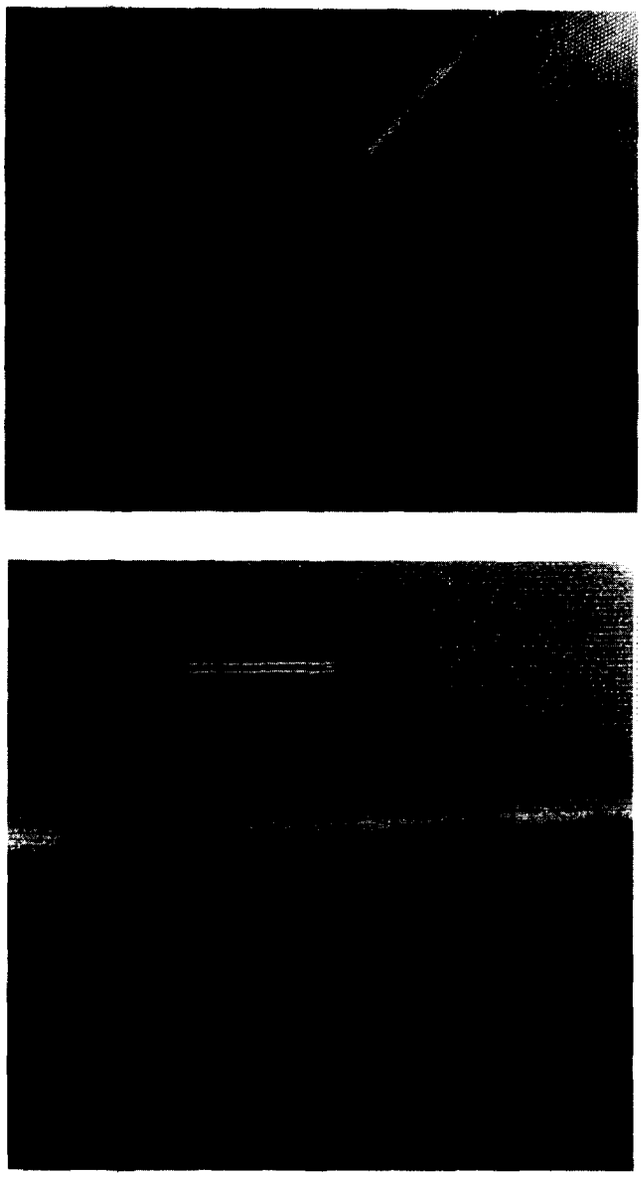

Fig. 11. (a) Curved grain boundary containing thin amorphous film. The arrow points towards the centre of curvature. (b) High resolution TEM image of the grain boundary region. Ledges can be observed on the {10$\bar{1}$0} facets. The lattice fringes in the two adjacent β'-grains correspond to the {10$\bar{1}$0} planes with a spacing of 0·66 nm.

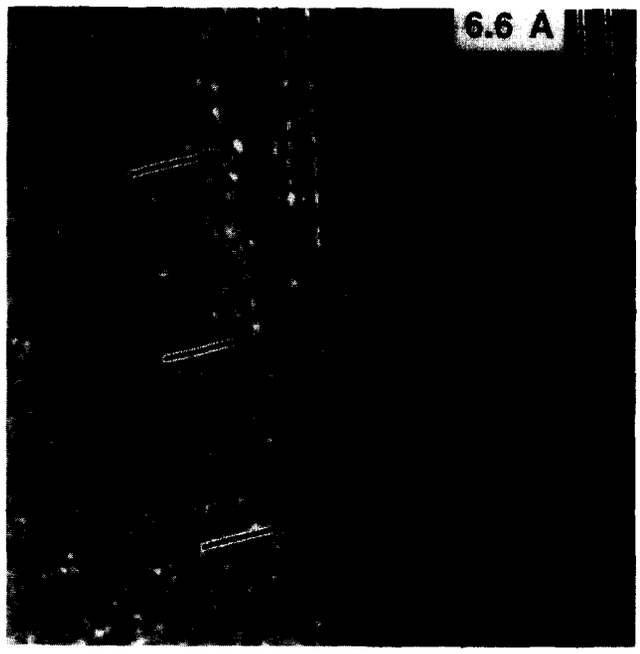

Fig. 12. Extremely thin grain boundary film separating two adjacent β'-grains. Ledges (arrowed) can be observed on the {10$\bar{1}$0} facets. The lattice fringes correspond to the {10$\bar{1}$0} planes with a spacing of 0·66 nm.

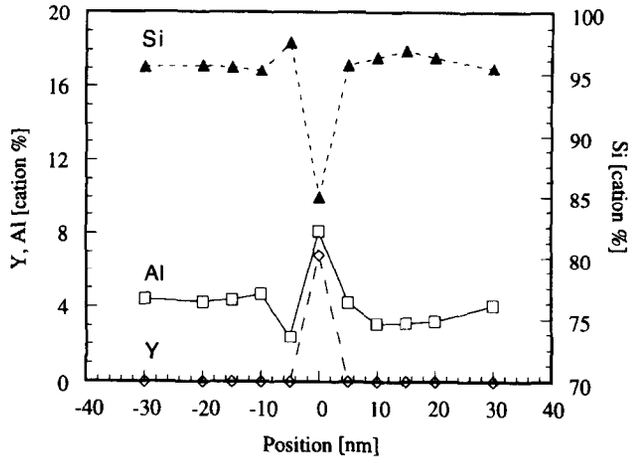

Fig. 13. Cation concentration profiles across the extremely thin glassy grain boundary film in Fig. 13.

4 Discussion

The metal oxide composition of the starting powder compact corresponded to that of the Y,Al-garnet (YAG) with an Y/Al atomic ratio of 0·6. Incorporation of Al into the Si_3N_4 during the densification process reduced the Al concentration in the liquid to a level which was too low for the formation of YAG. The Al-substituted N-α-wollastonite (Y_2SiAlO_5N) instead formed during cooling through partial devitrification of the glass.[7] The Y/Al ratios of the analysed residual glass pockets were in the range 1·5–2·4 and the glass had a fairly high Si content, around 70 to 80 cation %. The high Si content as well as too low Y/Al ratios would suppress the formation of wollastonite. A continued β'-grain growth into glassy pockets would thus push the composition of the residual glass towards the wollastonite composition which indicates that a prolonged time at the densification temperature may result in an increased crystallisation of the residual glass during cooling. This is consistent with results from X-ray diffraction presented in Ref. 1; prolonged time at densification temperature resulted in an increased volume fraction of Y_2SiAlO_5N.

Results discussed in Ref. 1 implied that β'-grain growth in this experimental material was rate controlled by diffusion through the liquid phase. A continued grain growth requires access to adequate amounts of Si and N, and Y and most of the Al and O which are not incorporated into

the β' structure have to diffuse away from the moving interface into the remaining liquid volume. This would result in the observed higher Y and Al concentrations of the glass close to the β'-grains. The grain growth rate would hence be influenced by the self diffusivity of the oxynitride liquid phase constituents at the densification temperature.

The observations that the growth fronts of the β'-grains are curved or irregular in the [0001] direction, while the $\{10\bar{1}0\}$ facets are flat when they grow without interference is consistent with results from previous investigations.[9] The rounded interfaces would allow faster growth in the [0001] direction by providing kink sites on the more rough surface while the flat $\{10\bar{1}0\}$ sides grow more slowly. This would result in anisotropic grain growth and elongated grains.

Curved grain boundaries indicate β'-Si_3N_4 grain growth by coalescence as discussed in Ref. 1. A β'-Si_3N_4 grain would be preferentially dissolved where the intergranular film is most narrow due to the increased pressure. Dissolved species may then diffuse through the film and reprecipitate on the opposite β'-grain. The curvatures of the grain boundaries in Fig. 11 suggest that the ledges on the $\{10\bar{1}0\}$ facets are growth ledges; the boundary will move towards its centre of curvature during coalescense. Y and Al were detected also in extremly thin intergranular films (Fig. 13) which shows that the additives will influence the transport properties also of grain boundary films and, hence, grain growth by coalescence.

5 Conclusions

1. Al and O were incorporated into the Si_3N_4 structure whereby a dilute β'-Si_3N_4 formed during the densification process. Concentration gradients of Al were not observed within the β'-grains although the local Al substitution level varied.
2. Formation of β'-Si_3N_4 reduced the Al content of the oxynitride liquid phase sintering medium during densification. This resulted in the formation of N-α-wollastonite instead of the Y,Al-garnet corresponding to the metal oxide composition of the starting powder mixture.
3. Local variations in the chemistry of the residual glassy phase resulted from β'-Si_3N_4 grain growth. An enrichment of Y and Al was observed close to the β'-grains. Y and Al were detected also in thin glassy grain boundary films between adjacent β'-grains.
4. The β'-Si_3N_4 grains generally tend to grow as hexagonal prisms with planar prism sides but irregular or rounded growth fronts in the [0001] direction.
5. Growth ledges on $\{10\bar{1}0\}$ facets of β'-grains facing curved grain boundaries resulted in a variation of the amorphous intergranular film thickness. The film thickness was in one case determined to vary from 0·7 to 1·5 nm. Curved grain boundaries with growth ledges imply β'-grain growth by coalescence.

Acknowledgements

This project was supported by the Swedish Research Council for Engineering Science (TFR). The experimental material was fabricated at the Japan Fine Ceramics Center (JFCC), Nagoya, by Dr Kent Rundgren from the Swedish Ceramic Institute (SCI).

References

1. Björklund, H., Falk, L. K. L., Rundgren, K. and Wasén, J., β-Si_3N_4 grain growth, part I: Effect of metal oxide sintering additives. *J. Eur. Cer. Soc.*, 1997, **17**, 1287–1301.
2. Lange, F. F., Silicon nitride polyphase systems: Fabrication, microstructure and properties. *Int. Met. Rev.*, 1980, No. 1, 1–20.
3. Hampshire, S. and Jack, K. H., The kinetics of densification and phase transformation of nitrogen ceramics. In *Special Ceramics 7*, ed. D. Taylor and P. Popper. British Ceramic Research Association, Stoke-on-Trent, 1981, pp. 37–49.
4. Lewis, M. H. and Lumby, R. J., Nitrogen ceramics, liquid phase sintering. *Powder Metallurgy*, 1983, **26**(2), 73–89.
5. Lewis, M. H., Powell, B. D., Drew, P., Lumby, R. J., North, B. and Taylor, A. J., The formation of single-phase Si–Al–O–N ceramics. *J. Mater. Sci.*, 1977, **12**, 61–74.
6. Falk, L. K. L. and Dunlop, G. L., Crystallisation of the glassy phase in a Si_3N_4 material by post sintering heat treatments. *J. Mater. Sci.*, 1987, **22**, 4369–4374.
7. Jack, K. H., Sialons: A study in materials development. In *Non-Oxide Technical and Engineering Ceramics*, ed. S. Hampshire. Elsevier Applied Science, London, 1986, pp. 1–30.
8. Ekström, T. and Nygren, M., SiAlON ceramics. *J. Am. Ceram. Soc.*, 1992, **75**(2), 259–276.
9. Hwang, C. J. and Tien, T-Y., Microstructural development in silicon nitride ceramics. *Materials Science Forum*, 1989, **47**, 84–109.